IEEE Open Journal of
Industry Applications

Received 27 January 2021; revised 2 April 2021; accepted 12 April 2021. Date of publication 19 April 2021;
date of current version 10 May 2021. The review of this paper was arranged by Associate Editor Shafiq Odhano.

Digital Object Identifier 10.1109/OJIA.2021.3074028

Grid-Forming Converters: Control Approaches, Grid-Synchronization, and Future Trends—A Review

ROBERTO ROSSO [1] (Student Member, IEEE), XIONGFEI WANG [2] (Senior Member, IEEE), MARCO LISERRE [3] (Fellow, IEEE), XIAONAN LU [4] (Member, IEEE), AND SOENKE ENGELKEN [5] (Senior Member, IEEE)

(Invited Paper)

[1] WRD Wobben Research and Development GmbH, 26607 Aurich, Niedersachsen, Germany
[2] Energy Technology, Aalborg University, 9220 Aalborg, Denmark
[3] Chair of Power Electronics, Christian-Albrechts-Universitaet zu Kiel, 24143 Kiel, Schleswig-Holstein, Germany
[4] College of Engineering, Temple University, Philadelphia, PA 19122 USA
[5] WRD Wobben Research and Development, 28199 Bremen, Bremen, Germany

CORRESPONDING AUTHOR: ROBERTO ROSSO (e-mail: roberto.rosso@enercon.de)

ABSTRACT In the last decade, the concept of grid-forming (GFM) converters has been introduced for microgrids and islanded power systems. Recently, the concept has been proposed for use in wider interconnected transmission networks, and several control structures have thus been developed, giving rise to discussions about the expected behaviour of such converters. In this paper, an overview of control schemes for GFM converters is provided. By identifying the main subsystems in respect to their functionalities, a generalized control structure is derived and different solutions for each of the main subsystems composing the controller are analyzed and compared. Subsequently, several selected open issues and challenges regarding GFM converters, i. e. angle stability, fault ride-through (FRT) capabilities, and transition from islanded to grid connected mode are discussed. Perspectives on challenges and future trends are lastly shared.

INDEX TERMS Control structure overview, grid-forming converters, grid-following converters, power-synchronization.

I. INTRODUCTION

The concept of grid-forming (GFM) converters originally introduced for micro and islanded grid applications [1], [2], has been proposed as a viable solution for enhancing system stability and resiliency of wider interconnected power networks with high penetration of power electronics-based generation. The wider use of GFM converters gives rise to the need for a classification of the control approaches used to implement these types of converters, which are conceptually different from state-of-the-art grid-following (GFL) units.

This paper represents an extension of the work presented in [3], and its main objectives are described in the following. First the conceptual differences between GFM converters and state-of-the-art GFL converters are discussed. An overview of the control structures proposed in the literature for implementing GFM converters is presented, and once the main characteristics of this type of converter are identified, a generalized structure is proposed by splitting the control into subsystems with respect to their functionalities. Various solutions for each of the identified subsystems are then analyzed and compared, and the possible similarities as well as advantages/drawbacks of the examined approaches are critically reviewed.

The second part of the paper discusses the open issues and challenges of GFM converters. Since most of the reported GFM implementations are based on the power synchronization mechanism of synchronous machines (SMs), classical stability issues such as power angle stability may occur. Furthermore, due to the fact that GFM converters in contrast to state-of-the-art GFL units behave as voltage sources behind

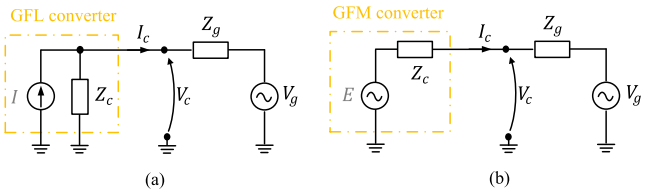

FIGURE 1. **(a) Simplified representation of a GFL converter, (b) simplified representation of a GFM converter [2].**

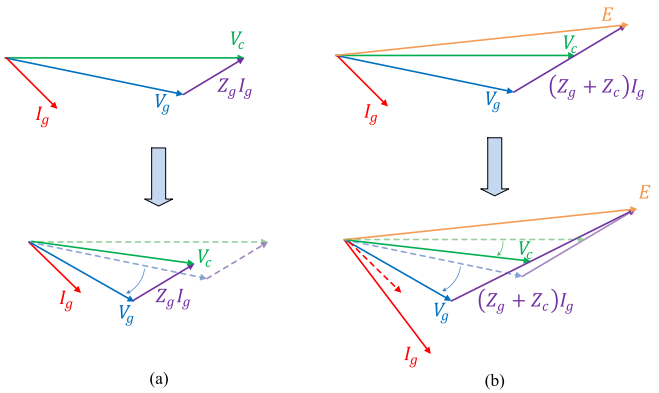

FIGURE 2. **(a) Phasor diagram of a GFL converter according to a perturbation of the grid voltage; (b) phasor diagram of a GFM converter according to a perturbation of the grid voltage.**

impedance, the currents of the GFM converter are determined by network conditions and may change rapidly. Therefore, proper fault ride-through (FRT) strategies should be adopted, in order to ensure the converter stability and prevent hardware damage. Additionally, while seamless transition from island condition to grid-connected mode has been intensively discussed in the last decade, this topic still represents a challenge for GFM converters. A comprehensive overview on the aforementioned aspects and open issues is provided in this paper. Finally, future trends regarding the specifications of GFM converters based on discussions at European level are reported.

The outline of the paper is the following: the main features of GFM converters compared to state-of-the-art GFL converters are discussed in Section II. A generalized structure is presented in Section III, where different solutions for each of the identified subsystems are presented and compared. In Section IV, challenges and open issues related to synchronization stability, FRT and transition from islanded to grid-connected mode of GFM converters are discussed, providing a comprehensive overview on the solutions reported in the literature. Finally, Section V is dedicated to the conclusions.

II. CONCEPTUAL DIFFERENCES BETWEEN GFM AND GFL CONVERTERS

There is no well-established formulation for the concept of GFM converters, and an official definition is currently under discussion in industrial and academic communities [4], [5]. Nevertheless, several GFM control structures have been proposed [6]–[19]. In [2], a GFL converter is described as a unit whose behavior can be approximated to a controlled current source with a high parallel impedance, whereas a GFM converter is represented as a voltage source with low series impedance. An example is shown in Fig. 1(a) and (b), where the common representations of a GFL and of a GFM converter are shown, respectively [2]. It is worth noting that this representation might erroneously resemble the definition of a Norton or a Thévenin equivalent, which are theoretically interchangeable; yet it does emphasize the fact that GFL converters achieve their purposes of power injection or voltage regulation by controlling the injected currents, while the GFM converter regulates the power by controlling directly the voltage at its output terminals. Additionally, the GFM converter under no-load conditions provides a reference voltage for the loads and the other units operating nearby, while the GFL converter necessarily requires a reference angle for the current injection.

In spite of different working principles, under steady-state operation, both GFM and GFL converters control active and reactive power injection into the grid according to the actual operating condition, while respecting the internal physical voltage and current limitations of the converter. Furthermore, both types of converters can achieve regulation of voltage and frequency at the connection point by means of additional outer loops, modifying actual active and reactive power setpoints, as usually required by grid codes [2], [20]. Nevertheless, the main differences among the two types of converters can be identified in the reaction to a grid event, and their small-signal behaviour under weak as well as stiff grid conditions.

Regarding the first aspect, Fig. 2 graphically explains the different reactions of the two different types of converters to a grid event. Because of its inherent current source behavior, the instantaneous reaction of the GFL converter is to maintain the current phasor $\mathbf{I}_g$ constant in terms of magnitude and phase, causing therefore an inevitable variation of the converter voltage phasor $\mathbf{V}_c$, due to the fact that the detection of the new phase angle of the phasor $\mathbf{V}_g$ is first needed in order to calculate the new current setpoint. Fig. 2 (b) describes the reaction of a GFM converter to the same event. According to its intrinsic behavior of a voltage source behind impedance, the internal voltage phasor $\mathbf{E}$ of the converter is initially not affected by the perturbation, causing an almost instantaneous variation of the phasor $\mathbf{I}_g$. Whilst this prompt reaction is surely superior to the one of a GFL unit, and it is thus highly attractive for system operators (SOs) [21], depending on the magnitude of the perturbation and on the characteristics of the system, this behavior might cause a rapid growth of the converter currents, hence jeopardizing the converter hardware components.

The second aspect characterizing the differences between GFM and GFL converters is related to their synchronization processes. A simplified representation of the working principles of the two examined converter types is reported in Fig. 3.

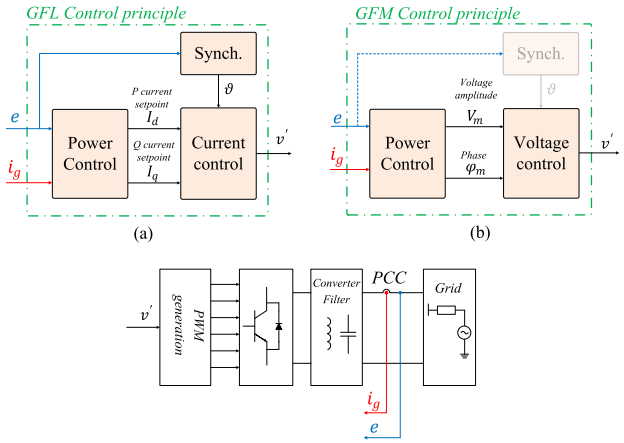

FIGURE 3. Simplified explanation of the control working principles: (a) GFL converter, (b) GFM converter.

It highlights the fact that, while a GFL converter requires a dedicated unit in order to identify the grid voltage angle and calculate a proper phase shift of the converter currents to inject the defined amount of active and reactive power, some of the GFM implementations proposed in the literature are able to self-synchronize to the grid without the need of a dedicated unit, but rather by emulating the power synchronization principle of a real SM [10]. To this extent, recent works have shown the negative effects of synchronization units, often implemented by means of phase-locked loops (PLLs), on the small-signal stability of grid-connected converters [22]–[25]. These studies demonstrate that, not only the stability margin of the single converter is reduced when other GFL converters operate in proximity to it, but additionally the interactions among the synchronization units of the converters operating nearby become stronger when decreasing the grid short-circuit ratio (SCR). In contrast to GFL converters, it has been shown in [26] and [27] that, due to their intrinsic behavior of a voltage source behind impedance, along with their ability of self-synchronization, GFM converters are instead suitable for weak grid applications. On the contrary, they result to be more prone to instability under stiff grid operating conditions compared to their counterpart GFL converters [28], [29], an aspect that will be further discussed in Section IV-A.

III. GENERAL STRUCTURE OF GFM CONTROL ALGORITHMS

In this section, an overview of the control structures of GFM converters is provided. Analyzing the GFM implementations presented in [6]–[19], a general formulation is first presented by identifying the main subsystems composing the control structure, along with their main functionalities. Subsequently, different implementations of each of the outlined subsystems are examined.

Fig. 4 shows the generalized control structure proposed in this paper. The measured three-phase converter currents, along with the currents and the voltages at the point of connection (PCC), indicated with i, i_g, and v, respectively, are among the control inputs of the converter. Further control inputs are the reference active power setpoint P^*, the reactive power setpoint Q^*, the reference frequency ω_{ref}, and the reference voltage V_{ref}. Two control loops are identified in the figure, and namely an outer control loop calculating the angle ϑ, the frequency ω, and the amplitude E_p of the inner virtual voltage source, and an inner current control loop, which instead includes all the further control actions that might take place in order to produce a proper modulation signal e' needed for PWM. In the following, different implementations for each of the subsystems composing the generalized control structure shown in Fig. 4 are discussed.

A. OUTER LOOP - POWER SYNCHRONIZATION LOOP

The power synchronization loop depicted in Fig. 4, contains two subsystems indicated as frequency loop and angle loop, and respectively in charge of the calculation of the frequency ω and the angle ϑ of the virtual inner voltage source. The interconnections between the two subsystems are not explicitly indicated in the figure, since these may differ according to the considered approach.

1) DROOP CONTROL

The simplest implementation of this subsystem is represented by the droop regulator depicted in Fig. 5 (a) [2], [6], [7], [9], whose mathematical expression is reported below:

$$\omega = \omega_{ref} + D_f(P^* - P) \tag{1}$$

with D_f indicating the droop coefficient, and representing the variation of the converter frequency according to the difference between active power setpoint P^* and the measured instantaneous power P. Then, the corresponding angle ϑ is obtained by integrating eq. (1). Though its simple structure, the droop control structure is very effective, and the use of an additional unit for synchronization purposes is not required during normal operation.

2) POWER SYNCHRONIZATION CONTROL (PSC)

While the droop regulator is a well-established technique for microgrid applications, the power synchronization control (PSC) proposed by Zhang *et al.* and presented in [10], represents the first control structure for grid-connected converters presented in the literature, overcoming the need for a dedicated synchronization unit. Initially proposed for HVDC applications, it has been developed in order to cope with the limitations of conventional vector controlled voltage source converters (VSCs) operating under weak grid conditions. Synchronization is achieved by emulating the power synchronization mechanism of a SM, thus by means of transient power transfer, and its control structure is depicted depicted in Fig. 5 (b). The subsystem is described by the following equation:

$$\vartheta = \frac{1}{s}\left[k_i(P^* - P)\right] + \vartheta_{ref} \tag{2}$$

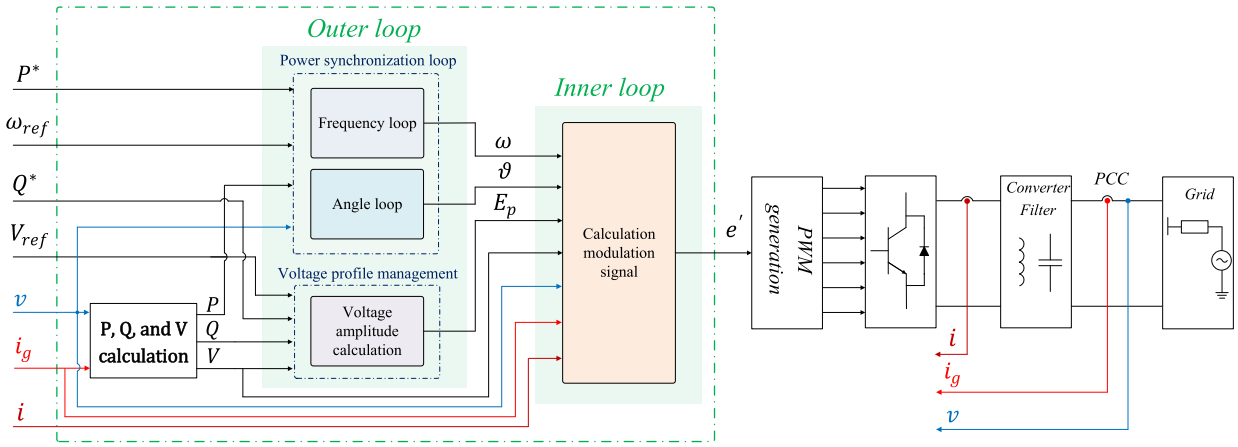

FIGURE 4. Generalized control structure of a GFM converter.

where k_i is a control parameter and ϑ_{ref} is obtained by integrating the reference signal ω_{ref}. Nevertheless, although a dedicated synchronization unit is not necessary for normal operation, a back-up PLL is employed for pre-synchronization purposes, as well as for operation during grid faults [10].

3) ENHANCED DIRECT POWER CONTROL (EDPC)

A similar structure as the one of the PSC can be found in [11], [12], and is shown in Fig. 5 (c). This has been labeled as enhanced direct power control (EDPC) and, in order to avoid switching form self-synchronization mode to PLL-mode during grid faults, the use of a PLL is foreseen also during normal operation. Indeed, the output frequency is continuously provided by the PLL, whereas the angle ϑ is calculated according to the following equation:

$$\vartheta = \left[P^* - P + \frac{1}{R_d}\left(\omega_{ref} - \omega_{PLL}\right)\right] G\left(1 + \frac{1}{Js}\right) + \vartheta_{PLL} \tag{3}$$

where a PI controller with gain G and time constant J is implemented. The parameter R_d represents the inverse of a frequency droop factor, whereas the time constant J acts as an additional degree of freedom for shaping the response of the converter according to a frequency variation, and provide a similar behavior as the one of a synchronous machine [11].

To this extent, the power synchronization loop of virtual synchronous machines (VSMs) is explicitly implemented so as to emulate the swing equation of a real SM, reported below for simplicity [30]:

$$J\dot{\omega} = T_m - T_e - D_f\omega \tag{4}$$

with J representing the moment of inertia, ω is the rotor speed, D_f is the mechanical friction, T_e is the electrical torque, and T_m is the mechanical one. This is the case of [8], [9], [14]–[18], and two of the most representative examples are reported in Fig. 5 (d) and (e).

4) SYNCHRONVERTER

The structure reported in Fig. 5 (d) is the synchronization loop of the VSM implementation known as synchronverter and presented in [13], [14]. It became very popular during the last decade, due to the fact that it can completely overcome the need for a synchronization unit both for pre-synchronization purposes, as well as and during normal operation. A sequence of switching actions is presented in [14], which, emulates the synchronization process of a real SM. Nevertheless, it is interesting to notice that the proposed synchronization process resembles the one of a standard PLL, as it has been mathematically demonstrated in [31]. The constant D_f indicated in the figure, not only represents the virtual damping factor of the control, but it also determines the steady-state droop behavior of the control. In order to compensate for the lack of this additional degree of freedom, modifications to the original synchronverter control structures have been proposed in the literature, so as to improve the dynamic response of the control while maintaining the same steady-state droop behavior [32]. The dashed branch in the figure, is introduced so as to activate or deactivate the droop control action of the converter, whose effects are canceled out by means of a PI controller. The expression of the angle ϑ calculated by the synchronverter, and including the dynamic of the PI control, is reported below:

$$\vartheta = \frac{1}{s}\left[\frac{(P^* - P)\frac{1}{J\omega_n}}{s + \frac{D_p}{J\left(1+D_pPI_p(s)\right)}} + \omega_{ref}\frac{\frac{D_p}{J\left(1+D_pPI_p(s)\right)}}{s + \frac{D_p}{J\left(1+D_pPI_p(s)\right)}}\right] \tag{5}$$

where $PI_p(s)$ indicates the transfer function of the PI control resulting from the chosen proportional and integral gain.

5) SYNCHRONOUS POWER CONTROL (SPC)

Finally, Fig. 5 (e) shows the power synchronization loop of the synchronous power control (SPC) presented in [15]-[16]. A second-order transfer function is implemented in the inner frequency loop, acting on the deviation between power setpoint P^* and measured power P. An additional frequency

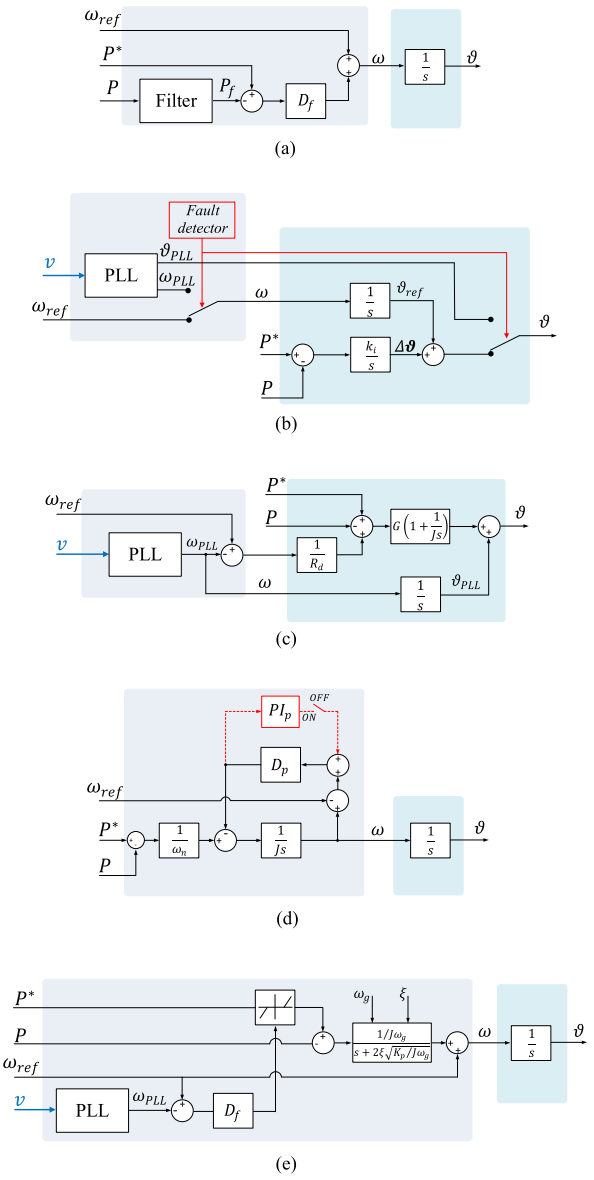

FIGURE 5. Power synchronization loop comparison: (a) frequency droop control [2], [6]–[7], (b) power synchronization control (PSC) [10], (c) enhanced direct power control (EDPC) [11], (d) synchronverter [13]–[14], (e) synchronous power control (SPC) [15], [16].

droop loop is also implemented, which modifies the active power setpoint according to the instantaneous deviation between ω_{ref} and the measured grid frequency ω, which can be for example estimated by means of a PLL. The expression of the angle ϑ calculated by the SPC is reported below:

$$\vartheta = \frac{1}{s}\left[\frac{(P^* - P)\frac{1}{J\omega_g}}{s + 2\zeta\sqrt{\frac{K_p}{J\omega_g}}} + \omega_{ref}\right] \tag{6}$$

where J is the virtual moment of inertia, ζ is a damping factor, and K_p represents the steady-state value of the transfer function between a variation of the converter angle $\Delta\vartheta$ and the injected converter power ΔP.

6) CONSIDERATIONS ABOUT THE EXAMINED STRUCTURES

Similarities among some of the structures examined above can be outlined. Apart from the possibility of obtaining an estimation of the grid frequency in the droop control according to eq. (1), and neglecting first the filtering of the measured power, the droop control of Fig. 5 (a) results to be identical to the PSC shown in Fig. 5 (b). Indeed, assuming $D_f = k_i$, the following equation is valid for both schemes:

$$\vartheta = \frac{1}{s}\left[D_f\left(P^* - P\right) + \omega_{ref}\right]. \tag{7}$$

The VSM with zero inertia constant (VSM0H) presented in [17]-[19] has basically the same control structure shown in Fig. 5 (a), where additionally the measured converter power P is processed by a boxcar filter with one cycle time constant. To this extent, it has been mathematically demonstrated in [9], that by properly filtering the measured converter power, the same inertial response of a VSM can be achieved with a droop controller.

Finally, the equivalence of the two synchronization loops of the VSM structures shown in Fig. 5 (d) and (e) has been proven in [33]. Indeed, by differentiating eq. (4) with respect to the power difference $P_{diff} = P^* - P$, yields for the synchronverter:

$$\frac{\partial\vartheta}{\partial P_{diff}} = \frac{1}{s}\left[\frac{\frac{1}{J\omega_n}}{s + \frac{D_p}{J}}\right]. \tag{8}$$

A similar calculation applied to eq. (6), gives the following result for the SPC:

$$\frac{\partial\vartheta}{\partial P_{diff}} = \frac{1}{s}\left[\frac{\frac{1}{J\omega_g}}{s + 2\zeta\sqrt{\frac{K_p}{J\omega_g}}}\right]. \tag{9}$$

As a consequence, the two expressions become equivalent when the control parameters of the two VSM implementations are chosen as follows:

$$J\omega_n = J\omega_g \quad ; \quad \frac{D_p}{J} = 2\zeta\sqrt{\frac{K_p}{J\omega_g}}. \tag{10}$$

B. OUTER LOOP - VOLTAGE PROFILE MANAGEMENT

Several implementations of the synchronization loop of a GFM converter have been discussed above, showing a relatively wide variety of possible choices. Regarding the subsystem in charge of the voltage regulation, the commonly adopted solutions can be summarized in three main categories: droop control, PI-based control, and cascaded controls involving droop and PI regulators. The considered schemes are shown in Fig. 6, and discussed in the following.

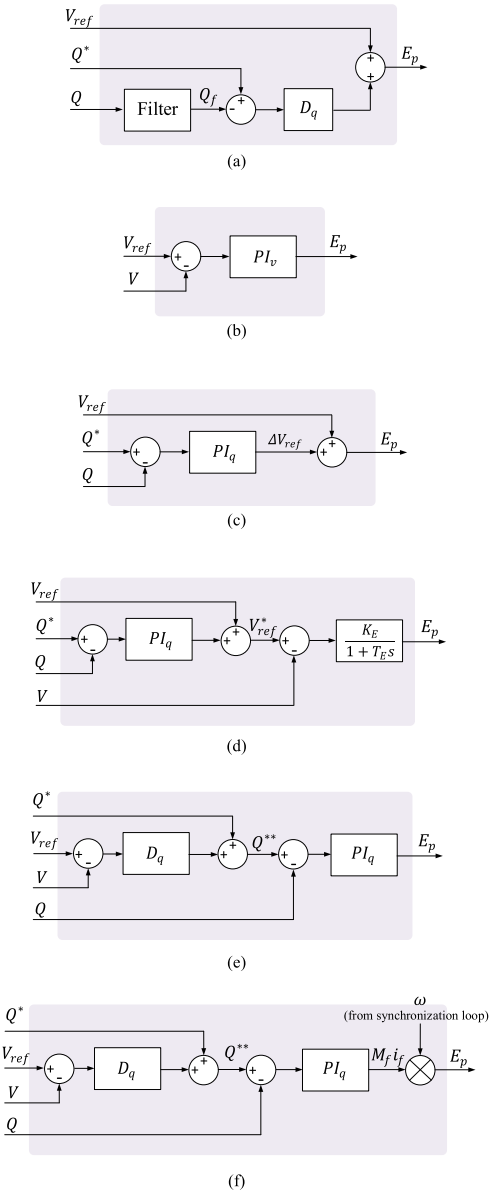

FIGURE 6. Different implementations of the voltage profile management loop: (a) droop control [1], [2], [7], [9], [18]; (b) PI-based voltage control for SPC [35]; (c) PI-based reactive power control for SPC [15], [16]; (d) cascaded structure with PI control in the first stage and droop in the second stage [10]; (e)-(f) cascaded structure with droop in the first stage and PI control in the second stage [11]–[14].

1) DROOP CONTROL

The first examined implementation is the droop control reported in Fig. 6 (a), which is usually adopted in combination with droop controllers in the synchronization loop [1], [2], [7], [9], [18]. In analogy to the droop structure shown in Fig. 5 (a), the filtering of the measured reactive power is explicitly introduced in the figure, as also indicated in [7]. The difference between the reactive power setpoint Q^* and the filtered measured power Q_f is processed through a proportional gain D_q. Subsequently, this quantity is added to the reference voltage V_{ref}, in order to calculate the amplitude of the inner voltage E_p of the GFM converter, thus the equation describing the implementation shown in Fig. 6 (a), is given below:

$$E_p = V_{ref} + D_q \left(Q^* - Q_f\right). \tag{11}$$

2) PI-BASED CONTROLLERS

The two schemes reported in Fig. 6 (b) and (c), represent PI-based solutions, which have been proposed for the implementation of the voltage profile management subsystem of the SPC. In the first case, a PI controller with transfer function PI_v regulates the amplitude of the measured voltage V at the PCC to the reference value V_{ref}, and has been presented in [35], for the implementation of a VSM-based Static Synchronous Compensator (STATCOM). In the second case, a PI controller with transfer function PI_q is implemented in order to regulate the reactive power Q to the setpoint Q^*, where, additionally, a feedforward of the reference voltage V_{ref} is included [15], [16]. The equations describing the two structures are reported below:

$$\begin{cases} E_p(s) = PI_v(s)\left(V_{ref} - V\right) & \text{(Fig. 6(b))} \\ E_p(s) = PI_q(s)\left(Q^* - Q\right) + V_{ref} & \text{(Fig. 6(c))} \end{cases}. \tag{12}$$

3) CASCADED CONTROLLERS

The schemes shown in Fig. 6 (d) and (e), represent two cascaded structures involving droop and PI controllers. The first implementation is the one adopted in the PSC [10], and consists of a PI controller in the outer stage, processing the reactive power difference, and an Alternating Voltage Controller (AVC) with a droop characteristic in the inner stage. The second implementation is instead widely adopted in the GFM literature [11]- [14], and consists of a droop controller in the first stage reacting to the voltage deviation, followed by a PI control in the second stage, the latter regulating the reactive power of the converter to the modified reactive power setpoint indicated in the figure with Q^{**}, which is calculated by adding to the signal Q^* the output of the droop regulator. The expressions describing the two formulations are reported below:

$$\begin{cases} E_p(s) = \left[PI_q(s)\left(Q^* - Q\right) + V_{ref} - V\right]\frac{K_E}{1+T_E s} & \text{(Fig. 6(d))} \\ E_p(s) = \left[D_q\left(V_{ref} - V\right) + Q^* - Q\right]PI_q(s) & \text{(Fig. 6(e))} \end{cases}. \tag{13}$$

In the specific case of the synchronverter, the structure is shown in Fig. 6 (f). Though conceptually similar to the one of Fig. 6 (e), the output of the PI controller represents a virtual mutual flux, indicated with $M_f i_f$. Hence, according to the scheme of Fig. 6 (f), E_p is calculated as [13], [14]:

$$E_p(s) = \left\{\left[D_q\left(V_{ref} - V\right) + Q^* - Q\right]PI_q(s)\right\}\omega \tag{14}$$

with ω the frequency calculated in the synchronization loop.

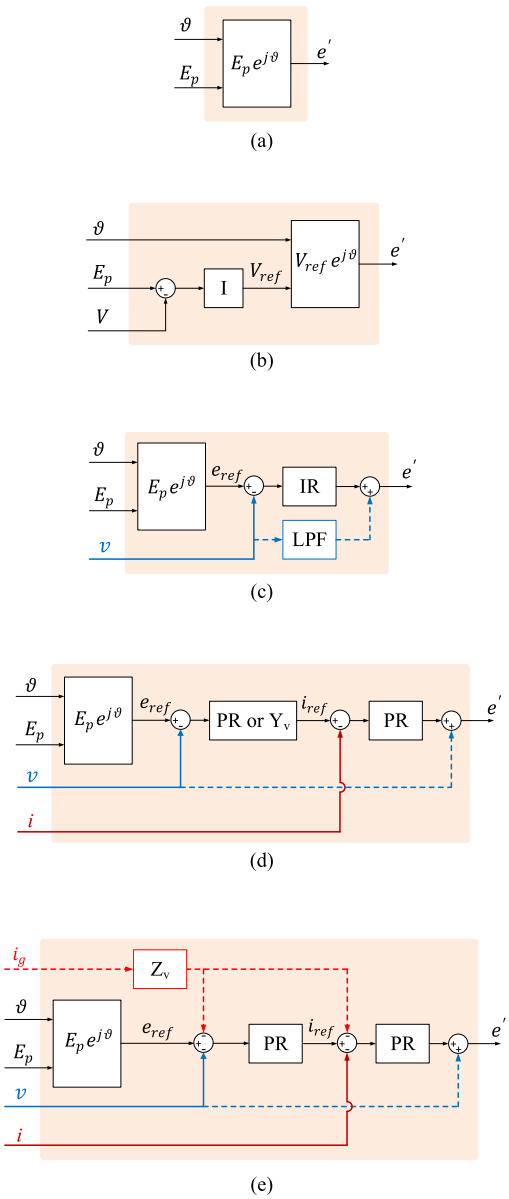

FIGURE 7. Block diagrams of voltage control loop for calculating the modulation signals. (a) Direct voltage synthesis [36], (b) voltage magnitude control [37], (c) single-loop voltage vector control [38], (d) dual-loop voltage vector control [42], (e) multi-loop voltage vector control with virtual impedance [47], [48].

C. INNER LOOP - CALCULATION OF THE MODULATION SIGNAL

A wide range of voltage control schemes have been developed for regulating the output voltage of GFM converters [36]-[46].

1) VOLTAGE VECTOR CONTROL

To regulate the output voltage waveform with high quality, the vector-voltage control can be implemented in a GFM converter, either with the single-loop or the multi-loop control structure. Fig. 7 (c) illustrates an example of single loop control diagram. The I + R (IR) controller is implemented in the $\alpha\beta$-frame [38], where the I controller is used for the additional 90° phase lag at high frequencies, and a high loop gain in the low-frequency range, while the R controller is designed for a zero steady-state tracking error at the fundamental frequency [40], [41]. Moreover, to further wide the stability region of the PR-I (or R) control, a two-degree-of-freedom control scheme is developed, indicated by the dashed line, and implemented by introducing a first-order low-pass filter (LPF) [41].

A major drawback of the single-loop voltage control is the lack of current controllability, which may cause the overcurrent tripping of the converter during grid faults. Hence, the dual-loop voltage and current control scheme is commonly used, as shown in Fig. 7 (d). It is composed by the inner filter inductor current control loop and the outer filter capacitor voltage control loop. The current loop serves two main purposes: 1) active damping of LC-filter resonance with the P controller, and 2) the prevention of overcurrent tripping with the I controller. Moreover, in the inner current loop, the I controller is generally tuned with a low gain in order not to affect the damping effect of the P controller at the LC-filter resonance frequency [42]. However, due to the time delay, a frequency-dependent virtual impedance, instead of a pure resistance, is added by the P current controller, and consequently, the control bandwidth of the outer voltage loop is still constrained [43]. Moreover, the control output impedance of the voltage loop exhibits a negative real part in the high-frequency range, which may destabilize the grid with high-frequency oscillations.

To enhance the performance of the dual-loop voltage control, the capacitor voltage is also fed back to the output of the inner current controller, known as the voltage feedback decoupling (VFD), which exhibits the higher control bandwidth and low frequency region of negative real part in the output impedance [44]. Fig. 8 (a) compares the inverter output impedance of the dual-loop voltage control without or with the VFD, which results in different stability under the same grid condition. This is demonstrated by means of the experimental results for the two examined cases reported in Fig. 8 (b) and (c) [38], [39], where single-phase converter currents before and after the capacitor filter are shown, indicated respectively with i_{1a} and i_{2a}, along with the capacitor voltage v_a, and the grid voltage v_{ga}.

2) MULTILOOP VECTOR CONTROL WITH VIRTUAL IMPEDANCE IMPLEMENTATION

Alternatively, the outer voltage controller can also be replaced by a virtual admittance [45], where the virtual admittance is designed as a first-order LPF. Instead of tracking the voltage reference with zero error, the virtual admittance provides more flexibility on shaping the output impedance of inverter [46].

Fig. 7 (e) illustrates the block diagram of the multi-loop vector-voltage control, where the grid current feed-forward loop is added in the dual-loop voltage and current control. The grid current feed-forward loop can be added at either the

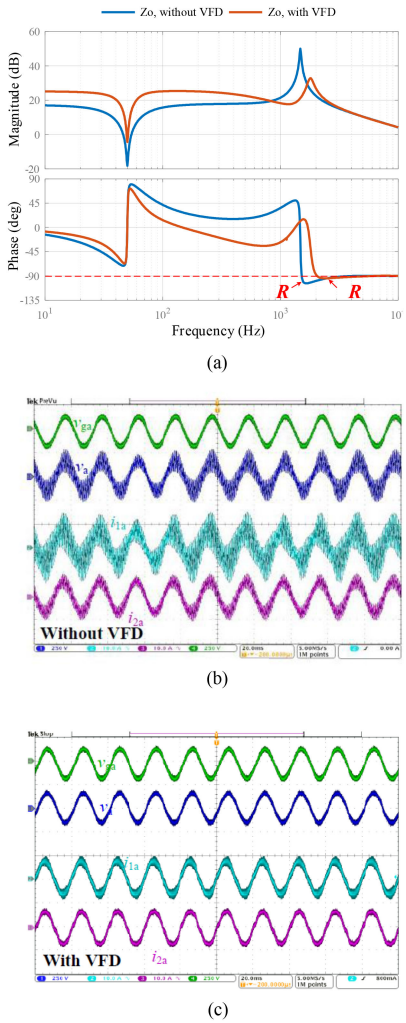

FIGURE 8. **(a) Output impedances of dual-loop control without or with voltage feedback decoupling (VFD). Stability results for the GFM converter with dual-loop voltage control under same grid condition: (b) without VFD, (c) with VFD [38].**

output or the input of the voltage regulator. With the different controllers, the grid current feed-forward loop can be used to synthesize various virtual impedances for the enhanced power control, active filtering, overcurrent limiting, etc. [47], [48].

D. VIRTUAL OSCILLATOR CONTROL (VOC)

Among the GFM implementations proposed in the literature, the concept of Virtual Oscillator Controls (VOCs) has gained interest in the last years within the research community. Based on a different working principle compared to the other synchronization strategies already examined in this section, it is discussed separately hereafter. Nevertheless, analogies to the structures previously examined are highlighted in the following, so that its implementation can still be subordinated to the the generalized structure presented in Fig. 4.

A VOC is a nonlinear control strategy, which makes a converter reproducing the dynamic of a weakly nonlinear limit-cycle oscillator. One of the most appealing characteristics related to this technique, is that it allows converters to synchronize with each other starting from an arbitrary initial conditions, without the need for any communication mean. An implementation for a single-phase converter in a microgrid application has been presented in [49], and [50]. Its structure is shown in Fig. 9 (a), and is succinctly discussed in the following. The employed oscillator model is the so-called Van der Pol oscillator, whose equations for the inductor current i_L and the capacitor voltage are given below [49]:

$$\begin{cases} L\frac{di_L}{dt} = v_c \\ C\frac{dv_c}{dt} = \sigma v_c - \alpha v_c^3 - i_L - k_i i \end{cases} \tag{15}$$

where the value of the resistance shown in the figure is $R = -\frac{1}{\sigma}$, while k_v and k_i are scaling factors for voltage and current, respectively. Hence, the modulation signal e' is directly calculated from the output capacitor voltage v_c properly scaled by a factor k_v. Thus, adopting the notation of Fig. 4, the following can be written [51]:

$$e' = k_v v_c(t) = E_p \cos(\vartheta) = E_p \cos(\omega_{ref} t + \Delta\vartheta). \tag{16}$$

Defining the following quantities:

$$\epsilon := \sqrt{\frac{L}{C}}, \quad \beta := \frac{3\alpha}{k_v^2 \sigma}, \quad g(y) := y - \frac{\beta}{3} y^3, \quad \omega_{ref} := \frac{1}{\sqrt{LC}}, \tag{17}$$

the oscillator dynamic is described by the following equations:

$$\begin{cases} \dot{E}_p = \omega_{ref}\epsilon\left(\sigma\ g\left(E_p cos(\omega_{ref} t + \Delta\vartheta)\right) - k_v k_i i\right) \\ \qquad\qquad \times cos(\omega_{ref} t + \Delta\vartheta) \\ \dot{\Delta\vartheta} = -\frac{\omega_{ref}\epsilon}{E_p}\left(\sigma\ g\left(E_p cos(\omega_{ref} t + \Delta\vartheta)\right) - k_v k_i i\right) \\ \qquad\qquad \times sin(\omega_{ref} t + \Delta\vartheta) \end{cases} \tag{18}$$

Though it can be demonstrated that by properly choosing control parameters of a VOC this can behave as a classical droop controller [50], one of the claimed advantages of a VOC lies on the fact that its working principle is based on instantaneous time-domain signals, rather than phasorial electrical quantities. Hence, superior performances of VOCs compared to classical droop controllers are expected. To this extent, the work presented in [51] compares the behaviour of droop controllers and a VOC for a three-phase converter in a micorgrid application. The considered control scheme is reported in Fig. 9 (b), which is identical to the scheme reported in Fig. 9 (a), with the only difference that the two signals $k_v v_c$, along with $\epsilon k_v i_L$ are employed as the $\alpha\beta$ components of the modulation signal e'. The results presented in [51], demonstrate a better dynamic behaviour of the VOC compared to a droop control when the frequency regulation range is higher than a certain threshold, however resulting in an opposite trend for a small frequency regulation range.

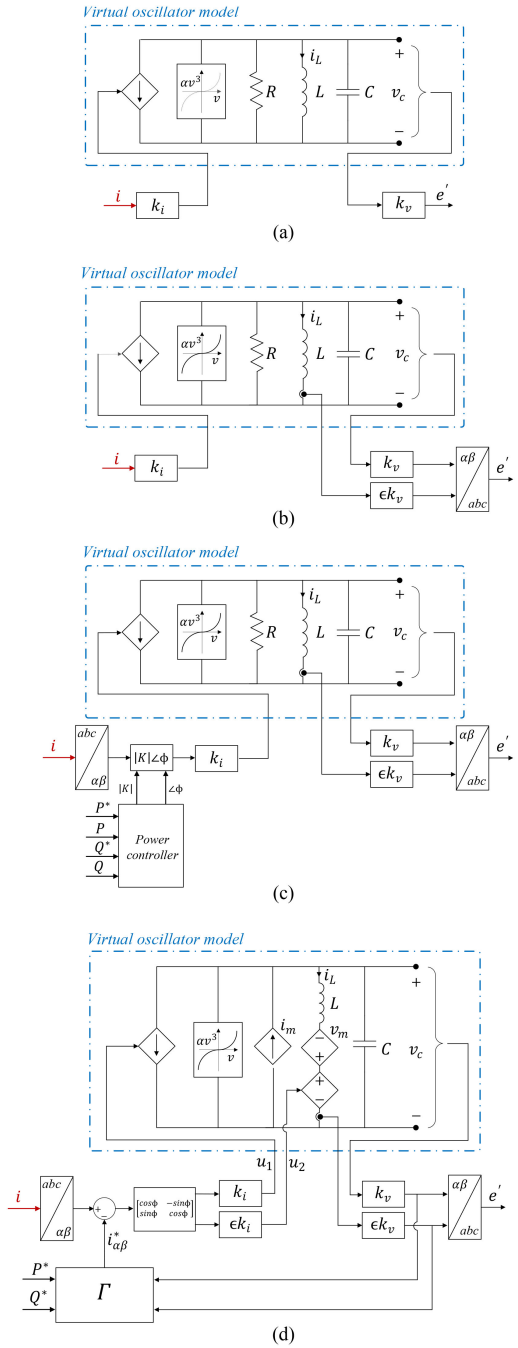

FIGURE 9. (a) VOC based on a Van der Pol oscillator for a single-phase converter [49], [50], (b) VOC based on a Van der Pol oscillator for a three-phase converter [51], (c) VOC based on a a Van der Pol oscillator with regulation of active and reactive power [54], (d) VOC based on a Andronov-Hopf oscillator with regulation of active and reactive power [55].

It is worth mentioning, that the VOC scheme proposed in [49]- [51] does not allow regulation of active and reactive power, becoming therefore not suitable for grid-connected applications. Thus, modifications to the original VOC based on the Van der Pol oscillator have been presented in [52] and [53], where a dispatchable VOC (dVOC) has been proposed, as well as in [54], where the control of active and reactive power is achieved by means of the control scheme shown in Fig. 9 (c). In the latter, a multiplication of the measured converter currents i with a complex factor $K = |K|\angle\phi$ permits the modification of the magnitude and the phase of the input current of the virtual oscillator, while the quantities $|K|$ and ϕ are calculated by means of a power control loop, so as to enable the regulation of the converter output power to the given setpoint.

Finally, Fig. 9 (d) shows the control scheme proposed in [55], which emulates the dynamic of so-called Andronov-Hopf systems. The considered virtual oscillator model is described by the following equations [55]:

$$\begin{cases} L\frac{di_L}{dt} = v_c + v_m - \epsilon u_2 \\ C\frac{dv_c}{dt} = -i_L + i_m - u_1 \end{cases} \tag{19}$$

where v_m and i_m are:

$$\begin{cases} v_m = \frac{\xi}{\omega_{ref}}(2\left(\frac{V_{ref}}{k_v}\right)^2 - \|x\|^2)\epsilon i_L \\ i_m = \frac{\xi}{\epsilon\omega_{ref}}(2\left(\frac{V_{ref}}{k_v}\right)^2 - \|x\|^2)v_c \end{cases}. \tag{20}$$

In (20), V_{ref} is indicated in terms of its RMS value, ξ is a constant affecting the convergence speed to steady-state, and $\|x\|$ represents the euclidean norm of the state vector $x = [v_c\ \epsilon i_L]^T$. The dynamic of the output voltage vector $v_{\alpha\beta} = k_v[v_c\ \epsilon i_L]$ is given by:

$$\begin{bmatrix} \dot{v}_\alpha \\ \dot{v}_\beta \end{bmatrix} = \begin{bmatrix} \frac{\xi}{k_v^2}(2V_{ref}^2 - \|v_{\alpha\beta}\|) - \omega_{ref} \\ \omega_{ref}\frac{\xi}{k_v^2}(2V_{ref}^2 - \|v_{\alpha\beta}\|) \end{bmatrix} \begin{bmatrix} v_\alpha \\ v_\beta \end{bmatrix} - \frac{k_v k_i}{C}\begin{bmatrix} \cos(\phi) - \sin(\phi) \\ sin(\phi)\cos(\phi) \end{bmatrix}\begin{bmatrix} i_\alpha - i_\alpha^* \\ i_\beta - i_\beta^* \end{bmatrix} \tag{21}$$

where, similarly as done in [54], ϕ represents a parameter producing a phase shift of the input signals to the virtual oscillator in order to affect active and reactive power injection. The current setpoints i_α^* and i_β^* are instead calculated as:

$$\begin{bmatrix} i_\alpha^* \\ i_\beta^* \end{bmatrix} = [\Gamma]\begin{bmatrix} P^* \\ Q^* \end{bmatrix} = \frac{2}{3\|v_{\alpha\beta}\|^2}\begin{bmatrix} v_\alpha & v_\beta \\ v_\beta & -v_\alpha \end{bmatrix}\begin{bmatrix} P^* \\ Q^* \end{bmatrix}. \tag{22}$$

According to this implementation, and considering the notation adopted in (18), the dynamical model for E_p and the phase angle $\Delta\vartheta$ results:

$$\begin{cases} \dot{E}_p = \frac{\xi}{k_v^2}E_p\left(2V_{ref}^2 - E_p^2\right) + \\ \qquad -\frac{k_v k_i}{3C}\frac{2}{E_p}(sin(\phi)(Q - Q^*) + cos(\phi)(P - P^*)) \\ \Delta\dot{\vartheta} = -\frac{k_v k_i}{3C}\frac{2}{E_p^2}(sin(\phi)(P - P^*) + cos(\phi)(Q - Q^*)) \end{cases} \tag{23}$$

revealing how the choice of the parameter ϕ can affect the relation between P and Q versus ω and E_p.

Without loss of generality, the control structure of a VOC can be mapped in the form proposed in Fig. 4, as indicated in

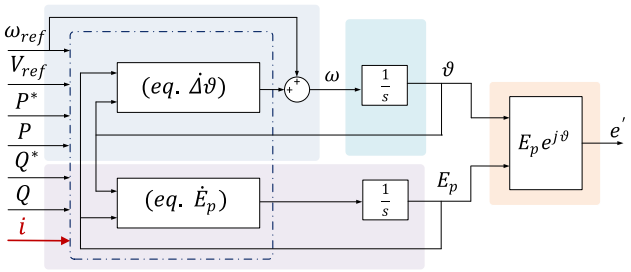

FIGURE 10. General VOC structure.

Fig. 10. In fact, independently on the considered VOC implementation among those examined in this section, the equations of the VOC are represented by a set of two non-linear differential equations for E_p and $\Delta\theta$, as it is the case of the Van der Pol-type oscillator investigated in [49]- [51] (eq. (18)), or the Andronov-Hopf-based structure issued in [55] (eq. (23)).

IV. OPEN ISSUES AND FUTURE TRENDS

In this section, open issues related to the implementation of GFM converters are discussed, providing a comprehensive overview on the solutions proposed in the literature.

A. SYNCHRONIZATION STABILITY

Keeping synchronism with the power network is essential to grid-connected converters. It has been observed that the use of a PLL with current control may reduce the stability margin of GFL converters in very low SCR grids [22], [25], [56]. This is because the converter tends to synchronize with the PCC voltage, which is highly affected by its output current in low SCR grids (see Fig. 1 (a) for a better illustration). This synchronization process introduces a negative damping to the grid [56].

In contrast, GFM converters synchronize with the grid based on their output active power, which is similarly to synchronous generators (SGs), as already discussed in the previous section. Differing from the PLL, this power-based synchronization, together with the PCC voltage control, allows the GFM converters to keep synchronism in low SCR grids [10]. However, in stiff grids with high SCRs, GFM converters tend to lose synchronism with the grid, since the slight change of the phase difference between the converter and grid voltages can lead to large active power variations [28], [29]. A more robust damping control is thus demanded for converters operating in a wide range of SCR conditions [57].

Besides the small-signal dynamic impact of synchronization control, the transient stability of GFM converters, i.e. the ability of converters to keep synchronism under large system disturbances, has also attracted increasing attention [58]-[65]. The droop-based power synchronization control (PSC-VSC) introduced in [10], exhibits a superior transient stability performance, due to its first-order nonlinear dynamic behavior [62]. With this control method, the system can be kept

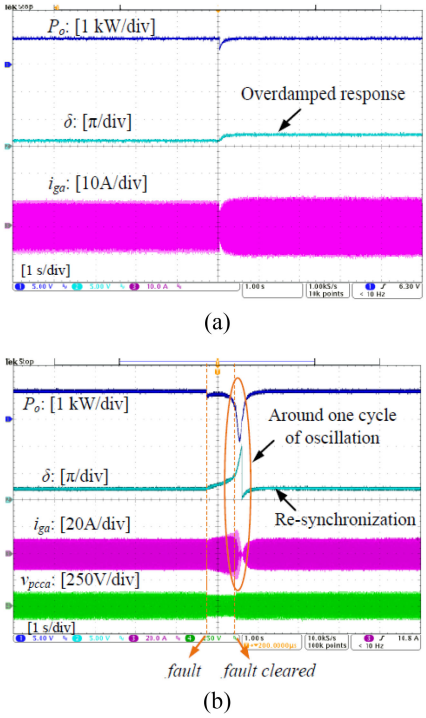

FIGURE 11. Experimental results of the dynamic responses of the VSC with power synchronization control during large transient disturbances. (a) With equilibrium points. (b) Without equilibrium points, and the fault clearing time > CCT [62].

stable whenever there are equilibrium points after the disturbance. Furthermore, when there are no equilibrium points, e.g. during severe grid faults, the critical fault clearing time (CCT) can be explicitly calculated. Yet, the power synchronization control with the virtual inertia exhibits a second-order nonlinear dynamic behavior, and consequently, its transient stability is similar to the power-swing dynamic of SGs [60]. It is worth mentioning that the overcurrent limiter of GFM converters may be triggered during severe grid faults, and the fault current of converters is usually controlled by the inner current loop, which is synchronized by the PLL [10]. The PLL thus becomes critical for the transient stability in such a scenario [63]. The commonly used dq-frame PLL is basically a second-order nonlinear system [64], whose transient stability impact has been found similar to the power-swing dynamic of synchronous generators [65]. Thus, a design-oriented analysis is performed to improve the transient stability of GFM converters during severe grid faults [63].

As an example, Fig. 11 (a) shows the experimental results of the dynamic responses of the PSC-VSC during large transient disturbances [62], where its overdamped response can be clearly observed. Thus, the transient instability does not occur for the PSC-VSC as long as it has equilibrium points after the disturbance. Moreover, for the severe faults without any equilibrium points, the PSC-VSC is able to automatically re-synchronize with the power grid after around one cycle of oscillation, even if the fault clearing time is beyond the CCT,

as shown in Fig. 11 (b), hence reducing the risk of system collapse caused by the delayed fault clearance.

In addition, the inner control loop may also interact with the outer control loop, affecting the synchronization stability of GFM converters [66]-[69]. This is mainly because the timescale of inner control loop may be coupled with that of outer power and synchronization control loop, depending on either the grid strength [66], [67] or the used inner loop control method [68], [69]. It has been shown in [69] that the single-loop voltage magnitude control, as shown in Fig. 7(b), leads to a dynamic coupling with the outer power control, and such coupling can enhance the synchronization stability of GFM converters. Hence, the effect of inner control loop needs to be examined before directly treating it as a unity gain, i.e., using the phasor model for GFM converter [67] for analyzing the synchronization stability. A more comprehensive analysis on the effect of inner loop can be found in [68].

Finally, [70] investigates the transient stability behaviour of a dVOC implemented by means of the Hopf-based oscillator reported in Fig. 9 (d), and compares it against the behaviour of a conventional droop control implemented by means of the scheme of Fig. 5 (a), whose filter time constant has been chosen so as to reproduce a certain inertial behaviour. The results reported in the paper, emphasize the advantages of the overdamped response of the dVOC which, in contrast to the droop control with inertial behaviour, is able to re-synchronize after fault clearance even if the clearing time is beyond the CCT, leading to similar conclusions as in [62], for the case of a PSC-VSC.

B. CURRENT LIMITATION AND FAULT-RIDE THROUGH (FRT)

It has been highlighted in Section II that, due to the intrinsic behavior of a voltage source behind impedance, the occurrence of grid faults might easily provoke unwanted converter overcurrents in a GFM converter, with consequent risks for hardware damages. The easiest solution in order to overcome this critical operating condition in a GFM converter, is to switch to a vector controlled mode at the occurrence of a fault, as proposed in [10]–[11].

Contrary to standard current limitation techniques originally adopted for GFM converters in stand-alone applications, and achieved mainly by means of saturating the PI controllers of the cascaded control loops [71]–[73], it has been demonstrated that virtual impedances represent an effective alternative for ensuring converter stability and avoiding classical phenomena of "wind-up" or "latch up" [74]. In fact, although limiting the converter currents due to overload conditions or grid faults might seem relatively simple, ensuring the stability of a GFM converter under such operating conditions could instead become challenging, especially when operating in parallel to standard SMs [75]. The virtual impedance concept consists of limiting the converter reference voltage according to fictitious variable impedance, in order to avoid the generation of excessively high current reference signals for the inner current control loop, or simply limiting the magnitude of the reference voltage when a GFM control structure without an inner current control loop is implemented [13], [14], [76].

Investigations of FRT strategies for VSMs have been mainly concerning the synchronverter control structure [77], [78]. To this extent, [79] proposes the modification of the standard synchronverter control structure by adding a cascaded inner current reference generator and an inner PI-based current control loop, in order to calculate proper converter currents out of the reference voltage signal during both normal conditions, as well as during balanced and unbalanced grid faults, according to the strategies proposed in [80]. Nevertheless, such solution does not allow fully exploiting the potentials of GFM converters during fault, which due to their emulated behaviour of voltage source behind impedance, are able of inherently injecting fault currents into the grid, without the need for an estimation of the type and magnitude of the fault.

Recent works have addressed the issues related to the instability of an outer control loop based on the power synchronization mechanism, and caused by the limitation of converter currents [81]– [83]. [81] investigates the implementation of a variable virtual impedance in order to increase the CCT, yet it does not explicitly avoid instability when the the fault is sustained. The work presented in [82], proposes a proper current limitation procedure, along with a coordination with the outer control loop, in order to prevent from the aforementioned instability phenomena, showing excellent results under symmetrical fault conditions. Finally, [83] proposes a current limitation strategy based on the limitation of the inner voltage of a GFM converter, in a similar manner as for the case of a variable virtual impedance, demonstrating the efficacy of the proposed approach also during asymmetrical faults.

Other works have presented strategies in order to directly control the converter currents of the converter, yet trying to ensure a GFM behaviour also during the fault [84]- [86]. These propose different ways for limiting positive and negative sequence current components of the GFM converters for the inner current control loop, in order to ensure stable operation, while preventing a GFM converter from the risk of hardware damages at the occurrence of a fault.

In Fig. 12 and Fig. 13, experimental results showing the FRT behaviour of a GFM converter adopting the control strategy proposed in [86], are reported, respectively for the case of a symmetrical and an asymmetrical grid fault. In the two figures, the reaction of the converter in terms of reactive power injection is highlighted, showing compliance with the draft grid codes for GFM converters elaborated in [87], which explicitly require a response of the converter within 5 ms after fault occurrence.

C. TRANSITION BETWEEN ISLANDED AND GRID-CONNECTED MODES

Transition between islanded and grid-connected operation modes could involve significant deviations and oscillations due to the potential mismatch in frequency and voltage amplitude (islanded mode to grid-connected mode) and non-zero

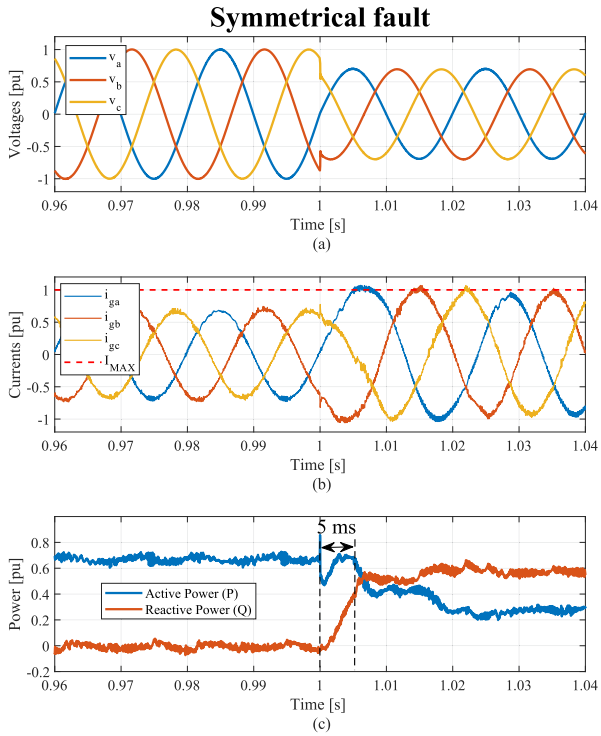

FIGURE 12. Experimental results showing the FRT behaviour of a GFM converter employing the control strategy proposed in [86]; symmetrical fault: (a) PCC voltages, (b) converter injected currents, (c) active and reactive power.

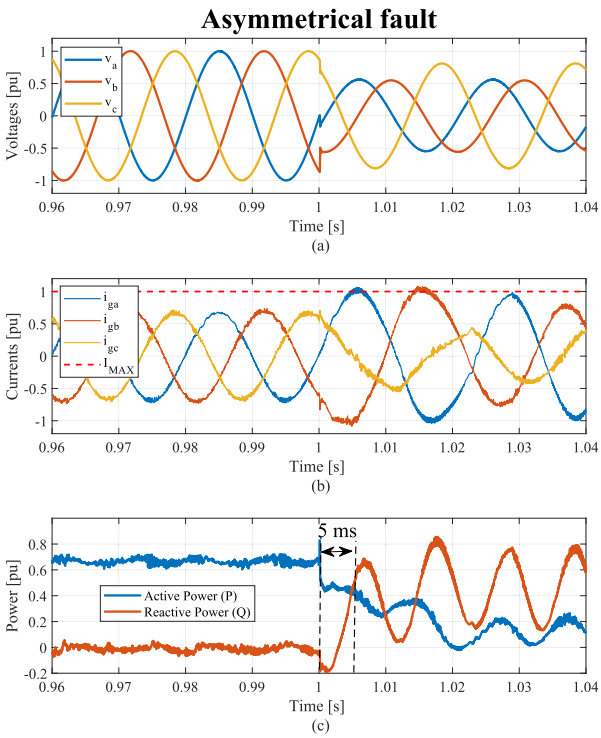

FIGURE 13. Experimental results showing the FRT behaviour of a GFM converter employing the control strategy proposed in [86]; asymmetrical fault: (a) PCC voltages, (b) converter injected currents, (c) active and reactive power.

through-power (grid-connected mode to islanded mode) [88]-[91]. GFM converters should handle both operation modes and ensure smooth transition between them. Particularly, under islanded operation mode, GFM converters should be able to automatically establish and stabilize system frequency and voltage, while under grid-connected mode, GFM converters should be controlled to inject specific amount of power in response to grid commands. More importantly, during the operation mode transition, it is necessary to avoid oscillations and instabilities and guarantee system stability in the pre-/post-transition operation.

In terms of the control approaches, droop control is widely adopted as the primary control of GFM converters, while seamless operation transition can be implemented in the secondary level [88], [89], [92]. The controller design is presented below:

$$\omega = \omega_{ref} + m(P - P^*) + \Delta\omega \tag{24}$$

$$E = V_{ref} - n(Q - Q^*) - \eta\, k_I \int (Q - Q^*)\, dt + \Delta E \tag{25}$$

where ω and E represent the converter operation frequency and voltage; ω_{ref} and V_{ref} represent the rated converter operation frequency and voltage; m and n represent the $P-f$ and $Q-V$ droop gains, respectively; P and Q represent the measured converter output active and reactve power P^* and Q^* represent the reference output active and reactive power under rated operation states; $\Delta\omega$ and ΔE represent the compensation terms involved by using secondary control; η indicates the converter operation mode, with $\eta = 1$ representing grid-connected mode, $\eta = 0$ representing islanded mode, and k_I is the integrator control gain.

The compensation terms involved by secondary control are introduced to ensure converter seamless operation mode switch. To seamlessly reconnect islanded GFM converters to the main grid, voltage phasors on both sides of the main breaker need to be synchronized; on the other hand, to seamlessly disconnect grid-connected GFM converters, through-power at the main breaker should be minimized before the system is islanded. These compensation terms are designed as:

$$\Delta\dot{\omega} = k_\omega(\omega_{ref} - \omega) + \lambda_R k_\vartheta \Delta\vartheta + \lambda_I k_P \Delta P \tag{26}$$

$$\Delta\dot{E} = (1 - \lambda_R)k_V(E - V_{ref}) + \lambda_R k_E \Delta E + \lambda_I k_Q \Delta Q \tag{27}$$

where $k\_$ represents the designed control gains; $\Delta\vartheta$ and ΔE represent the mismatch of voltage phase and magnitude across the main breaker during reconnection, and ΔP and ΔQ represent the through-power at the main breaker during disconnection; λ_R and λ_I as complementary binary variables indicate inverter operation mode, respectively, and $\lambda_R = 1$ indicates the converter is under regulation for seamless reconnection while $\lambda_I = 1$ represents planned disconnection.

Some simulation results are shown in Fig. 14, for operation mode transition of GFM converters. As shown in Fig. 14 (a), GFM converter is initially operated under islanded mode and

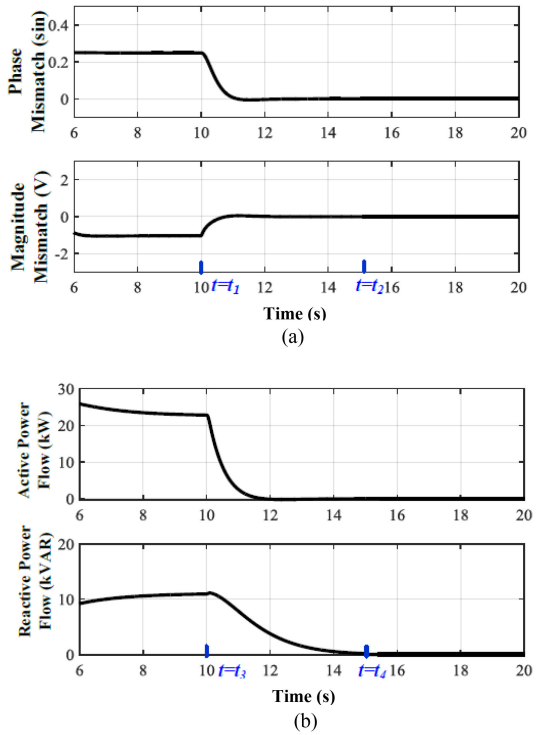

FIGURE 14. Operation mode transition of GFM converters. (a) Phase and voltage amplitude mismatch across the main breaker when transitioning from islanded mode to grid-connected mode. (b) Through-power at the main breaker when transitioning from grid-connected mode to islanded mode.

requested to reconnect to the main grid at $t = t_1$. The voltage phase and magnitude mismatch are eliminated at $t = t_2$ to perform a seamless reconnection as the main breaker closes. As shown in Fig. 14 (b), the GFM converters is initially operated under grid-connected mode and requested to switch to islanded mode at $t = t_3$. The through-power (active and reactive power) is minimized at $t = t_4$ to seamlessly island the system.

It is noteworthy that the seamless transition between grid-connected and islanded modes of GFM converters can be applied to particular applications in distribution systems and microgrids when the penetration of power electronics-based resources increases. For example, it can be implemented in dynamic microgrids, which are microgrids with dynamic electric boundaries residing in distribution systems for enhancing hosting capacity of power electronics-based resources, as well as grid resiliency [88], [89], [94]. In dynamic microgrids, multiple GFM converters can switch between grid-connected and islanded operation following the basic GFM control (i.e., droop control) and secondary control for additional regulation in steady-state and transient process, following the rules in eq. (24)-(27).

D. FUTURE TRENDS

The numerous amount of studies showing the potentials of GFM converters and their capability of stabilizing a power system with high penetration of power electronics-based generation [95], have triggered discussions in different countries, as well as at European level, with SOs about the challenges and opportunities presented by the GFM technology. In 2017, the European Network of Transmission System Operators for Electricity (ENTSO-E) established a working group on "High Penetration of Power Electronic Interfaced Power Sources' (EG HPoPEIPS)," whose members represent the wind, solar, and HVDC industries, power system analysis and tool providers, consultants, academia, and SOs [96]. The British SO (NGESO) convened an Expert Group on VSM associated with the Grid Code Consultation (GC0100) in early 2018 [87].

At the present stage, the following capabilities of GFM converters are debated [96]: creating system voltage, contributing to fault level, contributing to system inertia, supporting system survival to allow effective operation of Load Frequency Demand Disconnection (LFDD) for rare system splits, prevent adverse control interactions, acting as a sink to counter harmonics and unbalance in system voltage. Sharing the desired capabilities among different units spread among the system is currently a topic of discussion, along with other open questions as what proportion of converter interfaced equipment should have the aforementioned capabilities, or where and when the capability needs to be available. The resulting specifications of GFM converters might in certain cases even evolve in an opposite direction compared to actual grid codes. E. g., requiring the contribution of GFM converters in mitigating harmonics and imbalances in the system, implies necessarily to revise the current requirements on power quality of grid connected converters.

Additionally, there is a common agreement that the development of suitable processes for testing and validating the capabilities of the GFM converters is a mandatory step to be taken. In fact, due to the low level of maturity of specifications on GFM characteristics, manufacturer, academia, and SOs are called on to agree on suitable benchmark systems with clearly defined test cases, in order to verify the capability of the developed controllers. This does not only concern the provision of suitable RMS or EMT simulation models, but eventually also clear indications for site testing, aiming at validation of performances and certification.

V. CONCLUSION

This paper discusses the concept of GFM converters for wide interconnected system applications and provides an overview of the most relevant implementations available in the literature. The conceptual differences between GFM converters and state-of-the-art GFL converters are first pointed out. Subsequently, according to a comprehensive literature overview, a general structure of a GFM converter is presented, identifying the main subsystems composing it with respect to their functionalities. The identified control loops are discussed in detail in the paper, and different approaches for their implementations are critically reviewed. Some of the most relevant challenges related to the implementation of GFM are highlighted and thoroughly addressed. The behavior of different

implementations of GFM converters during large transient disturbances has been treated. Furthermore, the FRT capability of GFM converters has been discussed in the paper, along with the importance of a proper current limitation strategy, and a comprehensive literature overview on the topic has been provided. Finally, the seamless transition from islanded to grid-connected mode typically required from GFM converters has been reviewed, and simulation results and references to the most relevant works on the covered topic have been reported. The paper is concluded presenting the future trends for specifications of GFM converters currently debated by SOs at European level.

REFERENCES

[1] R. Lasseter, "Microgrids," in *Proc. Power Eng. Soc. Winter Meeting*, vol. 1, 2002, pp. 305–308.

[2] J. Rocabert, A. Luna, F. Blaabjerg, and P. Rodriguez, "Control of power converters in AC microgrids," *IEEE Trans. Power Electron.*, vol. 27, no. 11, pp. 4734–4749, Nov. 2012.

[3] R. Rosso, X. Wang, M. Liserre, X. Lu, and S. Engelken, "Grid-forming converters: An overview of control approaches and future trends," in *Proc. IEEE Energy Convers. Congr. Expo.*, Detroit, MI, 2020, pp. 4292–4299.

[4] M. Paolone *et al.*, "Fundamentals of power systems modeling in presence of converter-interfaced generation," *J. Electric Power Syst. Res.*, vol. 189, Dec. 2020, Art. no. 106811.

[5] J. Matevosyan *et al.*, "Grid-forming inverters: Are they the key for high renewable penetration?," *IEEE Power Energy Mag.*, vol. 17, no. 6, pp. 89–98, Nov./Dec. 2019.

[6] K. De Brabandere, B. Bolsens, J. Van den Keybus, A. Woyte, J. Driesen, and R. Balmans, "A voltage and frequency droop control method for parallel inverters," *IEEE Trans. Power Electron.*, vol. 22, no. 4, pp. 1107–1115, Jul. 2007.

[7] M. Chandorkar, D. M. Divan, and R. Adapa, "Control of parallel connected inverters in standalone ac supply systems," *IEEE Trans. Ind. Appl.*, vol. 29, no. 1, pp. 136–143, Jan. 1993.

[8] H.-P. Beck and R. Hesse, "Virtual synchronous machine," in *Proc. 9th Int. Conf. Elect. Power Qual. Utilization*, Oct. 2007, pp. 1–6.

[9] S. D'Arco and J. A. Suul, "Virtual synchronous machines classification of implementation and analysis of equivalence to droop controllers for microgrids," in *Proc. IEEE PowerTech*, 2013, Grenoble, France, Jun. 2013, pp. 1–7.

[10] L. Zhang, L. Harnefors, and H. P. Nee, "Power synchronization control of grid-connected voltage source converters," *IEEE Trans. Power Syst.*, vol. 25, no. 2, pp. 809–820, May 2010.

[11] M. Ndreko, S. Rüberg, and W. Winter, "Grid forming control for stable power systems with up to 100% inverter based generation: A paradigm scenario using the IEEE 118-bus system," in *Proc. 17th Int. Workshop Large-Scale Integration Wind Power into Power System (LSI)*, Sweden, Feb. 2018, pp. 16–18.

[12] M. Ndreko, S. Rüberg, and W. Winter, "Grid forming control for stable power systems with up to 100% power electronic interfaced generation: A case study on great britain test system," *IET Renewable Power Gener.*, vol. 14, no. 8, pp. 1268–1281, 2020.

[13] Q.-C. Zhong and G. Weiss, "Synchronverters: Inverters that mimic synchronous generators," *IEEE Trans. Ind. Electron*, vol. 58, no. 4, pp. 1259–1267, Apr. 2011.

[14] Q.-C. Zhong, P.-L. Nguyen, Z. Ma, and W. Sheng, "Self-synchronized synchronverters: Inverters without a dedicated synchronization unit," *IEEE Trans. Power Electron.*, vol. 29, no. 2, pp. 617–630, Feb. 2014.

[15] D. Remon, A. M. Cantarellas, E. Rakhshani, I. Candela, and P. Rodriguez, "An active power synchronization control loop for grid connected converters," in *Proc. IEEE PES Gen. Meeting*, Nat Harbor, MD, 2014, pp. 1–5.

[16] P. Rodriguez, C. Citro, I. Candela, J. Rocabert, and P. Rodriguez, "Flexible grid connection and islanding of SPC-based PV power converters," *IEEE Trans. Ind. Appl.*, vol. 54, no. 3, pp. 2690–2702, May/Jun. 2018.

[17] R. Ierna *et al.*, "Effects of VSM cenvertor control on penetration limits of non-synchronous generation in the GB power system," in *Proc. 15th Int. Workshop Large-Scale Integration Wind Power Power Syst.*, Vienna, 2016.

[18] A. J. Roscoe, M. Yu, A. Dysko, C. Booths, R. Ierna, and J. Zhu, "A VSM convertor control model suitable for RMS studies for resolving system operator/owner challenges," in *Proc. 15th Int. Workshop Large-Scale Integration Wind Power Power Syst.*, Vienna, 2016.

[19] M. Yu, "Framework for assessing stability challenges in future converter-dominated power networks," Ph.D. dissertation, Dept. Electron. Elect. Eng., Univ. Strathclyde, U.K., 2018.

[20] *IEEE standard for interconnection and interoperability of distributed energy resources with associated electric power systems interfaces* IEEE Standard. 1547, 2018.

[21] A. Johnson, "GC0100 - Fast Fault Current Injection, Fault Ride Through and Banding," [Online]. Available: https://www.nationalgrideso.com

[22] L. Harnefors, M. Bongiorno, and S. Lundberg, "Input-admittance calculation and shaping for controlled voltage-source converters," *IEEE Trans. Ind. Electron.*, vol. 54, no. 6, pp. 3323–3334, Dec. 2007.

[23] B. Wen, D. Boroyevich, R. Burgos, P. Mattavelli, and Z. Shen, "Analysis of DQ small-signal impedance of grid-tied inverters," *IEEE Trans. Power Electron.*, vol. 31, no. 1, pp. 675–687, Jan. 2016.

[24] J. Z. Zhou, H. Ding, S. Fan, Y. Zhang, and A. M. Gole, "Impact of short-circuit ratio and phase-locked-loop parameters on the small-signal behavior of a VSC-HVDC converter," *IEEE Trans. Power Del.*, vol. 29, no. 5, pp. 2287–2296, Oct. 2014.

[25] R. Rosso, M. Andresen, S. Engelken, and M. Liserre, "Analysis of the interaction among power converters through their synchronization mechanism," *IEEE Trans. Power Electron.*, vol. 34, no. 12, pp. 12321–12332, Dec. 2019.

[26] R. Rosso, J. Cassoli, G. Buticchi, S. Engelken, and M. Liserre, "Robust stability analysis of LCL filter based synchronverter under different grid conditions," *IEEE Trans. Power Electron.*, vol. 34, no. 6, pp. 5842–5853, Jun. 2019.

[27] R. Rosso, S. Engelken, and M. Liserre, "Robust stability analysis of synchronverters operating in parallel," *IEEE Trans. Power Electron.*, vol. 34, no. 11, pp. 11309–11319, Nov. 2019.

[28] Y. Liao, X. Wang, F. Liu, K. Xin, and Y. Liu, "Sub-synchronous control interaction in grid-forming VSCs with droop control," in *Proc. IEEE Workshop Electron. Grid (eGrid)*, Xiamen, China, 2019, pp. 1–6.

[29] X. Wang, M. G. Taul, H. Wu, Y. Liao, F. Blaabjerg, and L. Harnefors, "Grid-synchronization stability of converter-based resources—An overview," *IEEE Open J. Ind. Appl.*, vol. 1, pp. 115–134, 2020, doi: 10.1109/OJIA.2020.3020392.

[30] P. Kundur, *Power System Stability and Control*. New York, NY, USA: McGraw-Hill, 1994.

[31] Q. C. Zhong and D. Boroyevich, "Structural resemblance between droop controllers and phase-locked loops," *IEEE Access*, vol. 4, pp. 5733–5741, Sep. 2016.

[32] S. Dong and Y. C. Chen, "Adjusting synchronverter dynamic response speed via damping correction loop," *IEEE Trans. Energy Convers.*, vol. 32, no. 2, pp. 608–619, Jun. 2017.

[33] R. Rosso, S. Engelken, and M. Liserre, "A generalized formulation of active power synchronization based control algorithms for grid connected converters," in *Proc. IECON 44th Annu. Conf. IEEE Ind. Electron. Soc.*, Washington DC, USA, 2018, pp. 883–888.

[34] *VDE-Technische Anschlussregel Hochspannung (VDE-AR-N-4120)*.

[35] C. Li, R. Burgos, I. Cvetkovic, D. Boroyevich, L. Mili, and P. Rodriguez, "Analysis and design of virtual synchronous machine based STATCOM controller," in *Proc. IEEE 15th Workshop Control Model. Power Electron.*, Jun. 2014, pp. 1–6.

[36] B. T. Ooi and X. Wang, "Voltage angle lock loop control of the boost type PWM converter for HVDC application," *IEEE Trans. Power Electron.*, vol. 5, no. 2, pp. 229–235, Apr. 1990.

[37] R. H. Lasseter *et al.*, "CERTS microgrid laboratory test bed," *IEEE Trans. Power Del.*, vol. 26, no. 1, pp. 325–332, Jan. 2011.

[38] Y. Liao and X. Wang, "Evaluation of voltage regulators for dual-loop control of voltage-controlled VSCs," in *Proc. IEEE Energy Convers. Congr. Expo.*, Baltimore, MD, USA, 2019, pp. 5036–5042.

[39] Y. Liao, X. Wang, and F. Blaabjerg, "Passivity-based analysis and design of linear voltage controllers for voltage-source converters," *IEEE Open J. Ind. Electron. Soc.*, vol. 1, pp. 114–126, 2020, doi: 10.1109/OJIES.2020.3001406.

[40] Z. Li, Y. Li, P. Wang, H. Zhu, C. Liu, and F. Gao, "Single-loop digital control of high-power 400-Hz ground power unit for airplanes," *IEEE Trans. Ind. Electron.*, vol. 57, no. 2, pp. 532–543, Feb. 2010.

[41] X. Wang, P. C. Loh, and F. Blaabjerg, "Stability analysis and controller synthesis for single-loop voltage-controlled VSIs," *IEEE Trans. Power Electron.*, vol. 32, no. 9, pp. 7394–7404, Sep. 2017.

[42] P. C. Loh and D. G. Holmes, "Analysis of multiloop control strategies for LC/CL/LCL-filtered voltage-source and current-source inverters," *IEEE Trans. Ind. Appl.*, vol. 41, no. 2, pp. 644–654, Mar./Apr. 2005.

[43] Y. Geng, R. Yun, K. Chen, H. Wang, Bai, and X.Wu, "Parameters design and optimization for LC-type off-grid inverters with inductor-current feedback active damping," *IEEE Trans. Power Electron.*, vol. 33, no. 1, pp. 703–715, Jan. 2018.

[44] Z. Zou, G. Buticchi, and M. Liserre, "Analysis and stabilization of a smart transformer-fed grid," *IEEE Trans. Ind. Electron.*, vol. 65, no. 2, pp. 1325–1335, Feb. 2018.

[45] P. Rodriguez, I. Candela, C. Citro, J. Rocabert, and A. Luna, "Control of grid-connected power converters based on a virtual admittance control loop," in *Proc. 15th Eur. Conf. Power Electron. Appl.*, Lille, France, 2013, pp. 1–10.

[46] P. Rodriguez, I. Candela, and A. Luna, "Control of PV generation systems using the synchronous power controller," in *Proc. IEEE Energy Convers. Congr. Expo.*, Denver, CO, USA, 2013, pp. 993–998.

[47] X. Wang, Y. W. Li, F. Blaabjerg, and P. C. Loh, "Virtual-impedance-based control for voltage-source and current-source converters," *IEEE Trans. Power Electron.*, vol. 30, no. 12, pp. 7019–7037, Dec. 2015.

[48] Z. Zou, G. Buticchi, and M. Liserre, "Grid identification and adaptive voltage control in a smart transformer-fed grid," *IEEE Trans. Power Electron.*, vol. 34, no. 3, pp. 2327–2338, Mar. 2019.

[49] B. B. Johnson, M. Sinha, N. G. Ainsworth, F. Dörfler, and S. V. Dhople, "Synthesizing virtual oscillators to control islanded inverters," *IEEE Trans. Power Electron.*, vol. 31, no. 8, pp. 6002–6015, Aug. 2016.

[50] M. Sinha, F. Dörfler, B. B. Johnson, and V. Dhople, "Uncovering droop control laws embedded within the nonlinear dynamics of van der pol oscillators," *IEEE Trans. Control Netw. Syst.*, vol. 4, no. 2, pp. 347–358, Jun. 2017.

[51] Z. Shi, J. Li, H. I. Nurdin, and J. E. Fletscher, "Comparison of virtual oscillator and droop controlled islanded three-phase microgrids," *IEEE Trans. Energy Convers.*, vol. 34, no. 4, pp. 1769–1780, Dec. 2019.

[52] M. Colombino, D. Groß, J. Brouillon, and F. Dörfler, "Global phase and magnitude synchronization of coupled oscillators with application to the control of grid-forming power inverters," *IEEE Trans. Autom. Control*, vol. 64, no. 11, pp. 4496–4511, Nov. 2019.

[53] G. Seo, M. Colombino, I. Subotic, B. Johnson, D. Groß, and F. Dörfler, "Dispatchable virtual oscillator control for decentralized inverter-dominated power systems: Analysis and experiments," in *Proc. IEEE Appl. Power Electron. Conf. Expo.* (APEC), Anaheim, CA, USA, 2019, pp. 561–566.

[54] D. Raisz, T. T. Thai, and A. Monti, "Power control of virtual oscillator controlled inverters in grid-connected mode," *IEEE Trans. Power Electron.*, vol. 34, no. 6, pp. 5916–5926, Jun. 2019.

[55] M. Lu, S. Dutta, V. Purba, S. Dhople, and B. B. Johnson, "A grid-compatible virtual oscillator controller: Analysis and design," in *Proc. IEEE Energy Convers. Congr. Expo.*, Baltimore, MD, USA, 2019, pp. 2643–2649.

[56] D. Dong, B. Wen, D. Boroyevich, P. Mattavelli, and Y. Xue, "Analysis of phase-locked loop low-frequency stability in three-phase grid-connected power converters considering impedance interactions," *IEEE Trans. Ind. Electron.*, vol. 62, no. 1, pp. 310–321, Jan. 2015.

[57] L. Harnefors, M. Hinkkanen, U. Riaz, F. Rahman, and L. Zhang, "Robust analytic design of power-synchronization control," *IEEE Trans. Ind. Electron.*, vol. 66, no. 8, pp. 5810–5819, Aug. 2019.

[58] O. Göksu, R. Teodorescu, C. L. Bak, F. Iov, and P. C. Kjær, "Instability of wind turbine converters during current injection to low voltage grid faults and PLL frequency based stability solution," *IEEE Trans. Power Syst.*, vol. 29, pp. 1683–1691, Jul. 2014.

[59] H. Wu and X. Wang, "Transient angle stability analysis of grid converters with the first-order active power loop," in *Proc. IEEE Appl. Power Electron. Conf. Expo.*, San Antonio, TX, USA, 2018, pp. 3011–3016.

[60] D. Pan, X. Wang, F. Liu, and R. Shi, "Transient stability analysis of droop-controlled grid-connected converters with inertia-emulating low-pass filters," in *Proc. IEEE Energy Convers. Congr. Expo.*, Baltimore, MD, USA, 2019, pp. 34–40.

[61] Z. Shuai, C. Shen, X. Liu, Z. Li, and Z. J. Shen, "Transient angle stability of virtual synchronous generators using lyapunov's direct method," *IEEE Trans. Smart Grid.*, vol. 10, no. 4, pp. 4648–4661, Jul. 2019.

[62] H. Wu and X. Wang, "Design-oriented transient stability analysis of grid-connected converters with power synchronization control," *IEEE Trans. Ind. Electron.*, vol. 66, no. 8, pp. 6473–6482, Aug. 2019.

[63] H. Wu and X. Wang, "Design-oriented transient stability analysis of PLL-synchronized voltage-source converters," *IEEE Trans. Power Electron.*, vol. 35, no. 4, pp. 3573–3589, Apr. 2020.

[64] H. Geng, L. Liu, and R. Li, "Synchronization and reactive current support of PMSG based wind farm during severe grid fault," *IEEE Trans. Sustain. Energy*, vol. 9, no. 4, pp. 1596–1604, Oct. 2018.

[65] M. Taul, X. Wang, P. Davari, and F. Blaabjerg, "An overview of assessment methods for synchronization stability of grid-connected converters under severe symmetrical grid faults," *IEEE Trans. Power Electron.*, vol. 34, no. 10, pp. 9655–9670, Oct. 2019.

[66] T. Qoria, F. Gruson, F. Colas, X. Guillaud, M. Debry, and T. Prevost, "Tuning of cascaded controllers for robust grid-forming voltage source converter," in *Proc. Power Syst. Comput. Conf.*, Dublin, Ireland, 2018, pp. 1–7.

[67] T. Qoria, F. Gruson, F. Colas, X. Kestelyn, and X. Guillaud, "Analysis of the coupling between the outer and inner control loops of a grid-forming voltage source converter," in *Proc. 22nd Eur. Conf. Power Electron. Appl. (EPE'20 ECCE Europe)*, Lyon, France, 2020, pp. P.1–P.10.

[68] M. Dokus and A. Mertens, "On the coupling of power-related and inner inverter control loops of grid-forming converter systems," in *IEEE Access*, vol. 9, pp. 16173–16192, 2021.

[69] T. Liu and X. Wang, "Transient stability of single-loop voltage-magnitude controlled grid-forming converters," *IEEE Trans. Power Electron.*, vol. 36, no. 6, pp. 6158–6162, Jun. 2021.

[70] H. Yu, M. A. Awal, H. Tu, I. Husain, and S. Lukic, "Comparative transient stability assessment of droop and dispatchable virtual oscillator controlled grid-connected inverters," *IEEE Trans. Power Electron.*, vol. 36, no. 2, pp. 2119–2130, Feb. 2021.

[71] M. A. Zamani, A. Yazdani, and T. S. Sidhu, "A control strategy for enhanced operation of inverter-based microgrids under transient disturbances and network faults," *IEEE Trans. Power Del.*, vol. 27, no. 4, pp. 1737–1747, Oct. 2012.

[72] N. Bottrell and T. C. Green, "Comparison of current-limiting strategies during fault ride-through of inverters to prevent latch-up and wind-up," *IEEE Trans. Power Electron.*, vol. 29, no. 7, pp. 3786–3797, Jul. 2014.

[73] W. Du, R. H. Lasseter and A. S. Khalsa, "Survivability of autonomous microgrid during overload events," *IEEE Trans. Smart Grid*, vol. 10, no. 4, pp. 3515–3524, Jul. 2019.

[74] J. He and Y. W. Li, "Analysis, design, implementation of virtual impedance for power electronics interfaced distributed generation," *IEEE Trans. Ind. Appl.*, vol. 47, no. 6, pp. 2525–2538, Nov./Dec. 2011.

[75] A. D. Paquette, and D. M. Divan, "Virtual impedance current limiting for inverters in microgrids with synchronous generators," *IEEE Trans. Ind. Appl.*, vol. 51, no. 2, pp. 1630–1638, Mar./Apr. 2015.

[76] V. Natarajan and G. Weiss, "Synchronverters with better stability due to virtual inductors, virtual capacitors, and anti wind-up," *IEEE Trans. Ind. Electron.*, vol. 64, no. 7, pp. 5994–6004, Jul. 2017.

[77] J. Alipoor, Y. Miura, and T. Ise, "Voltage sag ride-through performance of virtual synchronous generator," in *Proc. Int. Power Electron. Conf.*, Hiroshima, Japan, 2014, pp. 3298–3305.

[78] Z. Shuai, W. Huang, C. Shen, J. Ge, and Z. John Shen, "Characteristics and restrain method of fast transient inrush fault currents in synchronverters," *IEEE Trans. Ind. Electron.*, vol. 64, no. 9, pp. 7487–7497, Sep. 2017.

[79] T. Zheng, L. Chen, Y. Guo, and S. Mei, "Comprehensive control strategy of virtual synchronous generator under unbalanced voltage conditions," *IET Gener. Transmiss. Distrib.*, 2018, vol. 12, no. 7, pp. 1621–1630, 2018.

[80] R. Teodorescu, M. Liserre, and P. Rodriguez, *Grid Converters for Photovoltaic and Wind Power Systems*. NJ, USA: Wiley-IEEE Press, 2011.

[81] T. Qoria, F. Gruson, F. Colas, G. Denis, T. Prevost, and X. Guillard, "Critical clearing time determination and enhancement of grid-forming converters embedding virtual impedance ac current limitation algorithm," *IEEE Trans. Emerg. Sel. Topics Power Electron.*, vol. 8, no. 2, pp. 1050–1061, Jun. 2020.

[82] M. G. Taul, X. Wang, P. Davari, and F. Blaabjerg, "Current limiting control with enhanced dynamics of grid-forming converters during fault conditions," *IEEE Trans. Emerg. Sel. Topics Power Electron.*, vol. 8, no. 2, pp. 1062–1073, Jun. 2020.
[83] J. Chen, F. Prystupczuk, and T. O' Donnel, "Use of voltage limits for current limitations in grid-forming converters," *CSEE J. Power Energy Syst.*, vol. 6, no. 2, pp. 259–269, Jun. 2020.
[84] S. F. Zarei, H. Mokhtari, M. A. Ghasemi, and F. Blaabjerg, "Reinforcing fault ride through capability of grid forming voltage source converters using an enhanced voltage control scheme," *IEEE Trans. Power Del.*, vol. 34, no. 5, pp. 1827–1842, Oct. 2019.
[85] B. Mahamedi, M. Eskandari, J. E. Fletcher, and J. Zhu, "Sequence-based control strategy with current limiting for the fault ride-through of inverter-interfaced distributed generators," *IEEE Trans Sustain. Energy*, vol. 11, no. 1, pp. 165–174, Jan. 2020.
[86] R. Rosso, S. Engelken, and M. Liserre, "Current limitation strategy for grid-forming converters under symmetrical and asymmetrical grid faults," in *Proc. IEEE Energy Convers. Congr. Expo.*, Detroit, MI, 2020, pp. 3746–3753.
[87] NGESO, "Expert Group - Grid Supporting Fast Fault Current and Associated Control Including Virtual Synchronous Machine Approaches," [Online]. Available: https://www.nationalgrideso.com
[88] Y. Du, X. Lu, J. Wang, and S. Lukic, "Distributed secondary control strategy for microgrid operation with dynamic boundaries," *IEEE Trans. Smart Grid*, vol. 10, no. 5, pp. 5269–5282, Sep. 2019.
[89] Y. Du, X. Lu, J. Wang, and S. Lukic, "Dynamic microgrids with self-organized grid-forming inverters in unbalanced distribution feeders," *IEEE Trans. Emerg. Sel. Topics Power Electron.*, vol. 8, no. 2, pp. 1097–1107, Jun. 2020.
[90] T. L. Vandoorn, B. Meersman, J. D. M. De Kooning, and L. Vandevelde, "Transition from islanded to grid-connected mode of microgrids with voltage-based droop control," *IEEE Trans. Power Syst.*, vol. 28, no. 3, pp. 2545–2553, Aug. 2013.
[91] S. Lissandron and P. Mattavelli, "A controller for the smooth transition from grid-connected to autonomous operation mode," in *Proc. IEEE Energy Convers. Congr. Expo.*, Pittsburgh, PA, USA, 2014, pp. 4298–4305.
[92] J. Guerrero, J. C. Vasquez, J. Matas, L. G. de Vicuna, and M. Castilla, "Hierarchical control of droop-controlled AC and DC microgrids—A general approach toward standardization," *IEEE Trans. Ind. Electron.*, vol. 58, no. 1, pp. 158–172, Jan. 2011.
[93] Q. Shafiee, J. M. Guerrero, and J. C. Vasquez, "Distributed secondary control for islanded microgrids—A novel approach," *IEEE Trans. Power Electron.*, vol. 29, no. 2, pp. 1018–1031, Feb. 2014.
[94] Y. Du, X. Lu, J. Wang, B. Chen, H. Tu, and S. Lukic, "Dynamic microgrids in resilient distribution systems with reconfigurable cyber-physical networks," *IEEE Trans. Emerg. Sel. Topics Power Electron.*, to be published, doi: 10.1109/JESTPE.2020.2981921.
[95] MIGRATE, "The massive integration of power electronic devices," EU Project. [Online]. Available: https://www.h2020-migrate.eu/
[96] ENTSO-E, "High penetration of power electronic interfaced power sources (HPoPEIPS)," technical report, 2017. [Online]. Available: htttps://www.entsoe.eu

ROBERTO ROSSO (Student Member, IEEE) received the B.Sc. degree in electronic engineering and the M.Sc. degree in electrical engineering from the University of Catania, Catania, Italy, in 2009 and 2012, respectively. Since 2017, he has been working toward the Ph.D. degree in electrical engineering with the Christian-Albrechts-University of Kiel, Kiel, Germany.

In 2013, he joined the R&D Division of the wind turbine manufacturer ENERCON (Wobben Research and Development WRD), where he is currently with the Control Engineering Department. He is involved in several research projects addressing analytical models of electrical machines, control of electric drive systems, and control of grid-connected converters, contributing as an inventor and co-inventor to several patents held by the company.

His research focuses on converter control strategies for integration in systems with high penetration of power electronics-based power sources. He is Member of the Workgroup GC0137 established by the British System Operator NGESO on minimum specification required for provision of GB grid forming capability.

XIONGFEI WANG (Senior Member, IEEE) received the B.S. degree in electrical engineering from Yanshan University, Qinhuangdao, China, in 2006, the M.S. degree in electrical engineering from the Harbin Institute of Technology, Harbin, China, in 2008, and the Ph.D. degree in energy technology from Aalborg University, Aalborg, Denmark, in 2013.

Since 2009, he has been with the Department of Energy Technology, Aalborg University, where he became an Assistant Professor in 2014, an Associate Professor in 2016, a Professor and the Leader of Electronic Power Grid Research Program in 2018. Since 2020, he has also been a part-time Visiting Professor with the KTH Royal Institute of Technology, Stockholm, Sweden. His current research interests include dynamic analysis and control of power electronic converters and systems, power electronics for sustainable energy systems and electrical grids, high power converters, and multiconverter systems.

Dr. Wang is a Member-at-Large of Administrative Committee for the IEEE Power Electronics Society from 2020 to 2022, the Co-Editor-in-Chief of the IEEE TRANSACTION ON POWER ELECTRONICS, and an Associate Editor for the IEEE JOURNAL OF EMERGING AND SELECTED TOPICS IN POWER ELECTRONICS. In 2016, he was selected into Aalborg University Strategic Talent Management Program. He was the recipient of six Prize Paper awards in the IEEE transactions and conferences, the 2016 Outstanding Reviewer Award of the IEEE TRANSACTION ON POWER ELECTRONICS, the 2018 Richard M. Bass Outstanding Young Power Electronics Engineer Award from the IEEE PELS, the 2019 IEEE PELS Sustainable Energy Systems Technical Achievement Award, the 2020 IEEE Power & Energy Society Prize Paper Award, and the Highly Cited Researcher in the Web of Science in 2019 and 2020.

MARCO LISERRE (Fellow, IEEE) received the M.Sc. and Ph.D. degrees in electrical engineering from Bari Polytechnic, Bari, Italy, in 1998 and 2002, respectively. He was Associate Professor with Bari Polytechnic and since 2012, has been a Professor of reliable power electronics with Aalborg University, Aalborg, Denmark. Since 2013, he has been a Full Professor and the Chair of power electronics with Kiel University, Kiel, Germany. He has authored or coauthored 500 technical papers, which include 1/3 of them in international peer-reviewed journals, and a book. These works have received more than 35000 citations. In 2014, He was listed in ISI Thomson report The world's most influential scientific minds.

He has been awarded with an ERC Consolidator Grant for the project The Highly Efficient And Reliable smart Transformer, a new Heart for the Electric Distribution System.

He is a Member of IAS, PELS, PES, and IES. He is with these societies in different capacities. He was the recipient of the IES 2009 Early Career Award, the IES 2011 Anthony J. Hornfeck Service Award, the 2014 Dr. Bimal Bose Energy Systems Award, the 2011 Industrial Electronics Magazine Best Paper Award and the Third Prize paper award by the Industrial Power Converter Committee at ECCE 2012, 2012, 2017 IEEE PELS Sustainable Energy Systems Technical Achievement Award, and the 2018 IEEE-IES Mittelmann Achievement Award.

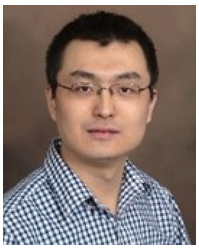

XIAONAN LU (Member, IEEE) received the B.E. and Ph.D. degrees in electrical engineering from Tsinghua University, Beijing, China, in 2008 and 2013, respectively. From September 2010 to August 2011, he was a Guest Ph.D. Student with the Department of Energy Technology, Aalborg University, Aalborg, Denmark. From October 2013 to December 2014, he was a Postdoc Research Associate with the Department of Electrical Engineering and Computer Science, University of Tennessee, Knoxville, TN, USA. From January 2015 to July 2018, he was with Argonne National Laboratory, Lemont, IL, USA, first as a Postdoc Appointee and then as an Energy Systems Scientist. In July 2018, he joined the College of Engineering, Temple University, Philadelphia, PA, USA, as an Assistant Professor. His research interests include modeling and control of power electronic inverters, hybrid and networked ac and dc microgrids, and real-time hardware-in-the-loop simulation.

Dr. Lu is an Associate Editor for the IEEE TRANSACTIONS ON INDUSTRIAL ELECTRONICS, IEEE TRANSACTIONS ON INDUSTRY APPLICATIONS, and the Editor of the IEEE TRANSACTIONS ON SMART GRID. He is the Vice Chair of the Industrial Power Converters Committee in the IEEE Industry Applications Society. He was the recipient of the 2020 Young Engineer of the Year Award in the IEEE Philadelphia Section.

SOENKE ENGELKEN (Senior Member, IEEE) received the B.Sc. degree in electrical engineering and computer science from Jacobs University Bremen, Bremen, Germany, in 2007, and the M.Sc. and Ph.D. degrees in control engineering from The University of Manchester, Manchester, U.K., in 2008 and 2012, respectively.

Since joining ENERCON's R&D division Wobben Research and Development in 2012, he has been occupied a number of technical and managerial positions, focusing on the development of control solutions for wind energy converters, spanning wind turbine controls, electrical systems controls, and grid-side converter controls. He is currently leading the R&D Transformation Office.

Dr. Engelken is a Member of the IEEE Power and Energy Society, IEEE Control Systems Society, and a past Member of the CIGRE Joint Working Group A1/C4.52 Wind Generators and Frequency-Active Power Control, and the ENTSO-E Expert Group on High Penetration Issues.